Results in Physics 11 (2018) 144–147

Contents lists available at ScienceDirect

Results in Physics

journal homepage: www.elsevier.com/locate/rinp

Novel Kerr-Vernier effects within the on-chip Si-ChG microring circuits

J. Ali[a], P. Youplao[b], N. Pornsuwancharoen[b], M.A. Jalil[c], M.S. Aziz[a], S. Chiangga[d], I.S. Amiri[e], S. Punthawanunt[f], G. Singh[g], P. Yupapin[h,i,*], K.T.V. Grattan[j]

[a] Laser Centre, IBNU SINA ISIR, Universiti Teknologi Malaysia, 81310 Johor Bahru, Malaysia
[b] Department of Electrical Engineering, Faculty of Industry and Technology, Rajamangala University of Technology Isan, Sakon Nakhon Campus, 199 Phungkon, Sakon Nakhon 47160, Thailand
[c] Physics Department, Faculty of Science, Universiti Teknologi Malaysia, 81310 Johor Bahru, Malaysia
[d] Department of Physics, Faculty of Science, Kasetsart University, Bangkok 10900, Thailand
[e] Division of Materials Science and Engineering, Boston University, Boston, MA 02215, USA
[f] Multidisciplinary Research Center, Faculty of Science and Technology, Kasem Bundit University, Bangkok 10250, Thailand
[g] Department of Electronics and Communication Engineering, Malaviya National Institute of Technology Jaipur, 302017, India
[h] Computational Optics Research Group, Advanced Institute of Materials Science, Ton Duc Thang University, District 7, Ho Chi Minh City, Viet Nam
[i] Faculty of Electrical & Electronics Engineering, Ton Duc Thang University, District 7, Ho Chi Minh City, Viet Nam
[j] Department of Electrical & Electronic Engineering, School of Mathematics, Computer Science & Engineering, City, University of London, EC1V 0HB, United Kingdom

A B S T R A C T

We propose a new concept of the nonlinear effect called the Kerr-Vernier effect by using cascaded Si-ChG microring circuits. The circuit is simulated for two materials of different refractive indices which results in phase difference in propagating light and hence observed in the output signal. By varying the input power into the system, the Vernier effects in terms of the Kerr-Vernier effects are seen. In application, the comparative results of the two-channel outputs are used to form the phase sensors, while the self-calibration between the two-channel outputs can be performed. The change in wavelength at the whispering gallery mode of 8 nm is achieved when the applied input power was fixed at 10 mW. A sensitivity of $\sim 120\,\mu m\,W^{-1}$ is obtained for this proposed sensor.

The Vernier effect is a well-known technique in coupled cavities passive systems to extend the free spectrum range (FSR) of band-pass filters. The Vernier effect is used in microring resonators photonics circuits to increase the FSR which in turns increase the capacity of the optical system thus contributing to embedding large channel count in DWDM system. It is widely used also for the design and fabrication of ultra-high performance telecommunication sensors. Vernier effect of the microring resonator may lead to a defect in the device fabrication which contributes to the error in light propagation phase and the overlapping in the output frequency comb [1]. However, the slight discrimination of the defect device from a required device can have the useful applications, for instance, for sensor applications [2–6]. There are the remarkable demonstrations on the Kerr switching in different materials found in the following Refs. [7–10]. By using the device called a Panda-ring resonator [11,12], the difference in the ring radii of two side rings introduces a similar Vernier effect as obtained by the defect device. However, the problem that it is difficult to overcome is the repeatability of the fabrication process. In this article, we have proposed that the ring radius is not required to change. Same results can be obtained by using the different ring materials or propagation lengths. The Vernier effect can be induced by nonlinear Kerr effect, which is known as the Kerr-Vernier effect. By varying the input power, nonlinear refractive index of the ring material with different lengths causes changes in the propagation of light and hence in output signals. The comparative output from two systems can be used for two-channel phase change measurements. It is the two-channel phase sensor that can be compared for self-calibration.

From Fig. 1, the electrical output field at the center ring is the electrical field of the whispering gallery mode ($\mathbf{E_{WGM}}$), which is given in the cylindrical coordinates and found in the Refs. [12,13]. To simplify the equation, reflection from the reflector is neglected, whereas the reflection output is obtained as $\mathbf{I_{WGMR}} = -\mathbf{R_{WGM}}\ \mathbf{I_{WGMR}}\cdot\ \mathbf{R_{WGM}}$. Here, $\mathbf{R_{WGM}}$ is the reflectance of the applied material [14]. Finally, the simulation parameters were selected closer to the considered practical parameters [15]. The parameters used in simulations are given in the captions of relevant figures. A selected light is fed into the system as the input electric field ($\boldsymbol{E_{in}}$). The electric fields are circulated within the system and described by the Eqs. (1) and (2) [16,17], the input electric field is fed into the z-axis, where $\boldsymbol{E_{in}} = \boldsymbol{E_Z} = \boldsymbol{E_0 e^{-ik_z z-\omega t+\varphi}}$, $\boldsymbol{E_0}$ is the initial electric field amplitude, Where $\boldsymbol{E_0}$ is the electric field amplitude

* Corresponding author at: Computational Optics Research Group, Advanced Institute of Materials Science, Ton Duc Thang University, District 7, Ho Chi Minh City, Viet Nam.
E-mail address: preecha.yupapin@tdtu.edu.vn (P. Yupapin).

https://doi.org/10.1016/j.rinp.2018.08.052
Received 11 April 2018; Received in revised form 28 August 2018; Accepted 29 August 2018
Available online 05 September 2018

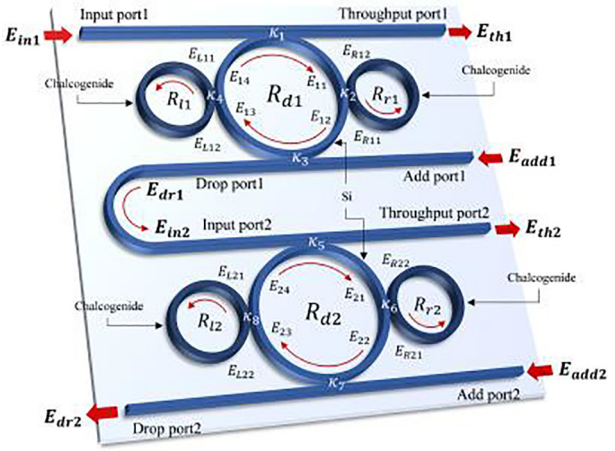

Fig. 1. A schematic of the on-chip Si-ChG microring circuits, where R_r, R_d, R_l are the ring radii of the center ring and two side rings, right (R_r) and left (R_l) hands, R_{Si}: silicon ring radius. E_{Subs} are the electrical fields in the related system.

(real), k_z is the wave number in the direction of propagation (z-axis), ω is the angular angular frequency, and is the initial phase.

The output intensity of the proposed single system is given by the transfer function of the output power (intensities) at through port and drop port given by Eqs. (1) and (2), respectively [17].

$$|E_{th}|^2 = \left|\frac{\tau_2-\tau_1 A\Phi}{1-\tau_1\tau_2 A\Phi}E_{in} + \frac{-\kappa_1\kappa_2 A_{1/2}\Phi_{1/2}}{1-\tau_1\tau_2 A\Phi}E_{ad}\right|^2 \quad (1)$$

$$|E_{dr}|^2 = \left|\frac{\tau_2-\tau_1 A\Phi}{1-\tau_1\tau_2 A\Phi}E_{ad} + \frac{-\kappa_1\kappa_2 A_{1/2}\Phi_{1/2}}{1-\tau_1\tau_2 A\Phi}E_{in}\right|^2 \quad (2)$$

where $A_{1/2}=e^{(-\alpha L/4)}$ is the half-roundtrip amplitude ($A = A_{1/2}^2$), $\Phi_{1/2} = e^{(j\omega T/2)}$ is the half-roundtrip phase contribution ($\Phi = \Phi_{1/2}^2$), $\tau_{1/2} = (1-\kappa_{1,2}^2)^{1/2}$, κ_1 and κ_2 are the coupling constants.

Before employing Eqs. (1) and (2) for simulations in MATLAB, preliminary results, as shown in Fig. 2, were obtained by using the graphical approach of the Optiwave program. Simulation of the laser input into the first system is illustrated in Fig. 1. The center wavelength is 1.55 μm with a peak power of 10 mW. A fraction of this power is coupled into the device that propagates throughout the first system and the output is obtained at the throughput port. Coupling constants and the other used parameters are given in the related figure captions. Next, the output from the drop port is input into the second system and the processes repeat.

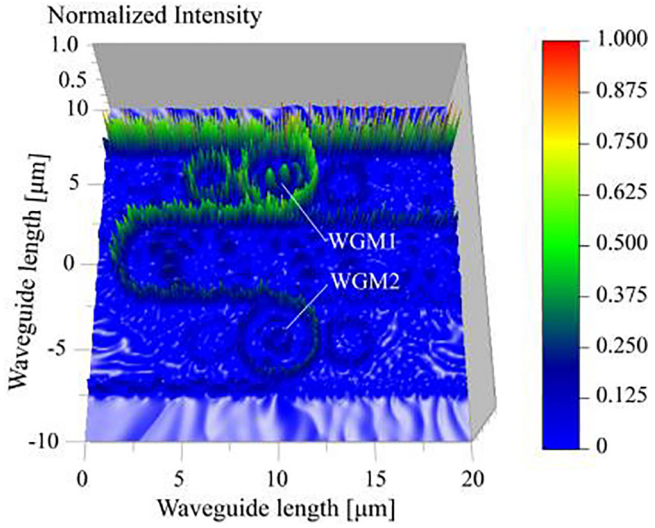

Fig. 2. The grapical results of the wave propagation in the system in Fig. 1 using the Optiwave program, where the input light source wavelength cenetr is at 1.55 μm, $R_{l1} = R_{r1} = R_{l2} = R_{r2} = 1.2$ μm, $R_{d1} = R_{d2} = 2.0$ μm, each of the coupling constant, κ_1 to κ_8 is 0.5, the refractive index; $n_{ChG} = 2.9$, $n_{Si} = 3.47$ (Si-Crystalline silicon).

The output of the second system is also obtained at the throughput port. In application, the two-channel sensor mechanism can be formed by the Kerr-Vernier effect within the circuits, which is firstly introduced by us in this work. In Fig. 2, the plot shows graphical results obtained from the Optiwave program, where the input light wavelength center is at 1.55 μm, $R_{l1} = R_{r1} = R_{l2} = R_{r2} = 1.2$ μm, $R_{d1} = R_{d2} = 2.0$ μm, each of the coupling constant, κ_1 to κ_8 is 0.5, the refractive index; $n_{ChG} = 2.9$ [18], $n_{Si} = 3.47$ (Si-Crystalline silicon).

The refractive index of Si is 3.47 The attenuation coefficient of the waveguide is 0.1 dB (mm)$^{-1}$, $A_{eff} = 0.50\,\mu m^2$. For simplicity, the waveguide loss is 0.5 for all wavelengths. The ChG dimension is given in the figure captions, the nonlinear refractive index $n_2 = 10.20 \times 10^{-18}\,m^2\,W^{-1}$ [20], linear refractive index $n_0 = 2.90$. The fractional intensity loss $\gamma = 0.1$ and other parameters are given in the related figure captions. The key parameter of such effects is the nonlinear refractive index (n_2) of the ChG, which is the side ring (phase modulator) that induces the coupling of power into the centre ring (Si). This affects the output at the throughput and drop ports. Hence, the less input power from drop port is coupled into the second system and observed at the throughput and drop ports, A different amount of power is coupled into the two side rings (right and left rings of both system) that provides with different refractive index changes induced by the Kerr effect. The shift in wavelength (or frequency) between the throughput ports of the systems introduce different phase changes due to the refractive index changes and produce two-channel comparative results. In a similar manner, the Vernier effect of the two side rings is reported by Bahadoran et al. [1]. This is the on-chip scale circuit that can be used for two-channel measurements, where the shifts of the two comparative results can offer better measurement accuracy, in which self-calibration can be performed. Regarding Kerr effect, the change in the input power causes the change in the output of Kerr-Vernier effects output, which is a display of a two-channel sensor operation.

The Kerr-Vernier effects of the system can be seen by changing the input power into the system, from which the output signal of the second system will be shifted in phase (wavelength). In the microring system, which is ultimately reflected in the refractive index, given by the relationship as $n = n_0 + n_2 I = n_0 + n_2 P/A_{eff}$, where n_0 and n_2 are the linear and nonlinear refractive indexes, respectively. I is the optical intensity and P is the optical power. A_{eff} is the effective mode core area of the device. For the microring resonator, the effective mode core areas range from 0.1 to 0.5 μm^2 [6]. The comparison of the results due to such effects is described in the following details. Fig. 3 shows the simulations performed using MATLAB and the two-channel comparative results at (a) through ports, (b) the drop ports, (c) the WGM outputs. In Fig. 4, the plot of the relationship between the input power and the changes in the output wavelengths with the two system outputs are compared, where the sensitivity of 1.2 W m^{-1} of the WGM output is obtained. In application, the initial measurement can be used as the off-set data before the sensing operation, therefore, if there is any change from the initial data will be the measurement values. Moreover, the shift in phase (optical path difference) from the two systems can be compared with each other, i.e. self-calibration. Moreover, the two-system can be used to form a sensor system in which one is the sensing unit and another one is performed the sensing unit, which has the potential of various sensor applications such as bio-sensors, mechanical sensors and other forms of sensor that requires the sensing and reference system comparison (see Table 1).

To the best of our knowledge, this is the first time the concept of the double effects called the Kerr-Vernier effects is introduced by using the material device size and refractive indices. The concept is demonstrated by using the two coupling panda-ring resonators, where the nonlinear

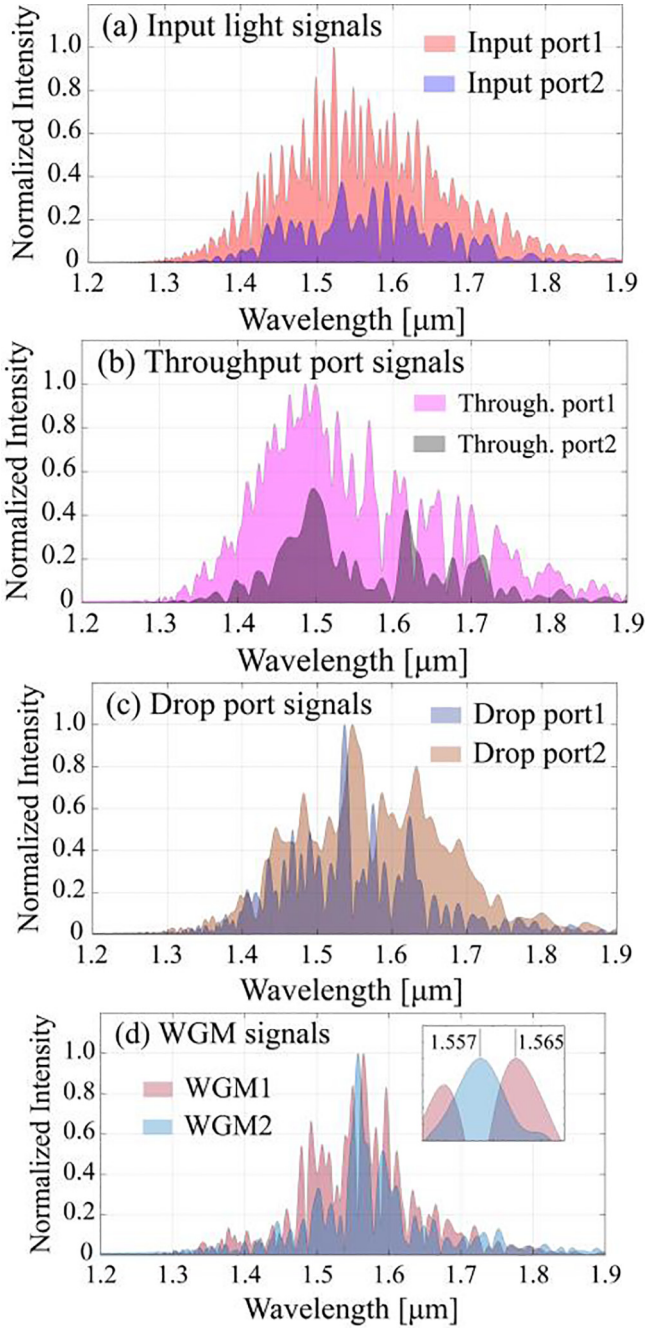

Fig. 3. Plot of the simulation results of the used parameters in Fig. 2 using the MATLAB program, where comparative results of the two-channel outputs at the (a) through ports, (b) the drop ports, (c) the WGM outputs. The through port signals present the Kerr-Vernier transmission outputs of the system.

material is the ChG. When light is input into the two systems, the Kerr effect is induced in both systems. By the difference in the propagation lengths, the longer length results in lower optical, which is observed by the phase differences. We have shown that the Kerr-Vernier effects within the microring resonator with the materials can be easily changed by applying the input power into the system, which is the external application. The comparison of the two outputs has shown that a phase shift of $\sim 120\,\mu m\,W^{-1}$ is obtained with an applied input power was fixed at 10 mW.

Acknowledgments

The authors would like to give the appreciation for the research financial support and the research facilities and financial support from the Universiti Teknologi Malaysia, Johor Bahru, Malaysia through Flagship UTM shine project (03G82), Tier 1 (16H44) and Tier 2 (15J57) grants.

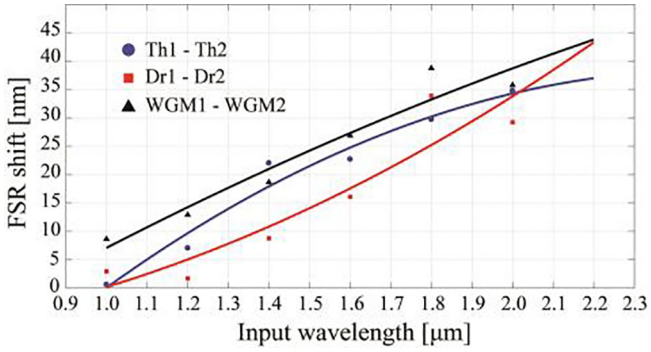

Fig. 4. The free spectrum range (FSR) of the output peak signals of the different input light sources from 1.0 to 2.0 μm. The plot ($\Delta\lambda/\lambda$) has shown the trend of linearity. The comparative results from (a) Th1 and Th2 in blue, (b) Dr1 and Dr2 in red, and (c) WGM1 and WGM2 in black, the data points and the solid lines are the simulation and the curve fitting point, respectively.

Table 1
Relative parameters of the Si-ChG microring system.

	R_{l1}, R_{l2}	R_{r1}, R_{r2}	R_{d1}, R_{d2}	Waveguide	κ_1-κ_8
Radius [μm]	1.2	1.2	2.0	–	–
A_{eff} [μm^2]	0.25	0.25	0.25	0.25	–
n_{Si}	–	–	3.47	3.47	–
n_0	2.9	2.9	–	–	–
n_{ChG} [m^2 W^{-1}]	10.2×10^{-18}	10.2×10^{-18}	–	–	–
Q [19]	$\sim 60^3$	$\sim 60^3$	$\sim 10^3$	–	–
Coupling ratio	–	–	–	–	0.5

Appendix A. Supplementary material

Supplementary data associated with this article can be found, in the online version, at https://doi.org/10.1016/j.rinp.2018.08.052.

References

[1] Sirawattananon C, Bahadoran M, Ali J, Mitatha S, Yupapin PP. Analytical Vernier effects of a Panda-ring resonator for microforce sensing application. IEEE Trans Nanotechnol 2012;11(4):707–12.
[2] Bahadoran M, Ali J, Yupapin PP. Ultrafast all-optical switching using signal flow graph for Panda resonator. Appl Opt 2013;52(12):2866–73.
[3] Bahadoran M, Ali J, Yupapin PP. Graphical approach for nonlinear optical switching by Panda Vernier filter. IEEE Photon Technol Lett 2013;25(15):1470–3.
[4] Sa-Ngiamsak W, Sirawattananon C, Srinuanjan K, Mitatha S, Yupapin PP. Micro-optical gyroscope using a Panda-ring resonator. IEEE Sens J 2012;12(8):2609–13.
[5] Chantanetra S, Teeka C, Mitatha S, Jomtarak R, Yupapin PP. Hybrid transistor manipulation controlled by light within a Panda microring resonator. IEEE Trans NanoBiosci 2012;11(2):125–30.
[6] Phatharaworamet T, Teeka C, Jomtarak R, Mitatha S, Yupapin PP. Random binary code generation using dark-bright soliton conversion control within a panda ring resonator. J Lightwave Technol 2010;28(19):2804–9.
[7] Wu CL, Su SP, Lin GR. All-optical modulation based on silicon quantum dot doped SiOx:Si-QD waveguide. Laser Photon Rev 2014;8(5):766–76.
[8] Wu CL, Lin YH, Su SP, Huang BJ, Tsai CT, Wang HY, et al. Enhancing optical nonlinearity in a nonstoichiometric SiN waveguide for cross-wavelength all-optical data processing. ACS Photon 2015;2(8):1141–54.
[9] Wu CL, Chen BT, Lin YY, Tien WC, Lin GR, Chiu YJ, et al. Low-loss and high-Q Ta_2O_5 based micro-ring resonator with inverse taper structure. Opt Express 2015;23(20):26268–75.
[10] Su SP, Wu CL, Cheng CH, Huang BJ, Wang HY, Tsai CT, et al. Nonstoichiometric SiC bus/ring waveguide based all-optical data format follower and inverter. ACS Photon 2016;3(5):806–18.
[11] Saktioto T, Irawan I, Yupapin P, Phatharacorn P. A single eye 3D image perception device using vertical double ring resonator construction. Microwave Opt Technol Lett 2015;57(8):1802–5.
[12] Phatharacorn P, Chiangga S, Yupapin P. Analytical and simulation results of a triple

micro whispering gallery mode probe system for a 3D blood flow rate sensor. Appl Opt 2016;55(33):9504–13.
[13] Ali J, Youplao P, Pornsuwancharoen N, Aziz MS, Chiangga S, Amiri IS, et al. On-chip remote charger model using plasmonic island circuit'. Results Phys 2018;9:815–8.
[14] Chaiwong K, Tamee K, Punthawanunt S, Suhailin FH, Aziz MS, Ali J, et al. Naked-eye 3D imaging model using the embedded micro conjugate mirrors within the medical micro-needle device. Microsyst Technol 2018;24(6):2695–9.
[15] Wang W, Chu ST, Little BE, Pasquazi A, Wang Y, Wang L, et al. Dual-pump Kerr micro-cavity optical frequency comb with varying FSR spacing. Sci Rep 2016;6:28501.
[16] Soysouvanh S, Jalil MA, Amiri IS, et al. Ultra-fast electro-optic switching control using a soliton pulse within a modified add-drop multiplexer. Microsyst Technol 2018;24(9):3777–37782.
[17] Amiri IS, Ali J, Yupapin PP. Enhancement of FSR and finesse using add-drop filter and panda ring resonator system. Int J Mod Phys 2012;B 26:1250034.
[18] Zakery A, Elliott SR. Optical nonlinearities in chalcogenide glasses and their applications, IX; 2007. 202 p., ISBN: 978-3-540-71066-0.
[19] Bogaerts W, Heyn PD, Vaerenbergh TV, Vos KD, Selvaraja SK, Claes T, et al. Silicon microring resonators. Laser Photon Rev 2012;6(1):47–73.
[20] Smektala F, Quemard C, Leneindre L, Lucas J, Barthélémy A, De Angelis C. Chalcogenide glasses with large non-linear refractive indices. J Non-Cryst Solids 1998;239(1–3):139–42.